

---

# Diagnosing Transformers: Illuminating Feature Spaces for Clinical Decision-Making

---

Aliyah R. Hsu<sup>1</sup>

Yeshwanth Cherapanamjeri<sup>1</sup>

Briton Park<sup>2</sup>

Tristan Naumann<sup>6</sup>

Anobel Y. Odisho<sup>4,5</sup>

Bin Yu<sup>1,2,3</sup>

<sup>1</sup> Department of Electrical Engineering and Computer Science, University of California, Berkeley

<sup>2</sup> Department of Statistics, University of California, Berkeley

<sup>3</sup> Center for Computational Biology, University of California, Berkeley

<sup>4</sup> Department of Urology, UCSF

<sup>5</sup> Department of Epidemiology and Biostatistics, UCSF

<sup>6</sup> Microsoft Research

## Abstract

Pre-trained transformers are often fine-tuned to aid clinical decision-making using limited clinical notes. Model interpretability is crucial, especially in high-stakes domains like medicine, to establish trust and ensure safety, which requires human engagement. We introduce SUFO, a systematic framework that enhances interpretability of fine-tuned transformer feature spaces. SUFO utilizes a range of analytic and visualization techniques, including Supervised probing, Unsupervised similarity analysis, Feature dynamics, and Outlier analysis to address key questions about model trust and interpretability. We conduct a case study investigating the impact of pre-training data where we focus on real-world pathology classification tasks, and validate our findings on MedNLI. We evaluate five 110M-sized pre-trained transformer models, categorized into general-domain (BERT, TNLN), mixed-domain (BioBERT, Clinical BioBERT), and domain-specific (PubMedBERT) groups. Our SUFO analyses reveal that: (1) while PubMedBERT, the domain-specific model, contains valuable information for fine-tuning, it can overfit to minority classes when class imbalances exist. In contrast, mixed-domain models exhibit greater resistance to overfitting, suggesting potential improvements in domain-specific model robustness; (2) in-domain pre-training accelerates feature disambiguation<sup>1</sup> during fine-tuning; and (3) feature spaces undergo significant sparsification during this process, enabling clinicians to identify common outlier modes among fine-tuned models as demonstrated in this paper. These findings showcase the utility of SUFO in enhancing trust and safety when using transformers in medicine, and we believe SUFO can aid practitioners in evaluating fine-tuned language models for other applications in medicine and in more critical domains.<sup>2</sup>

## 1 Introduction

Pre-trained transformer models achieve state-of-the-art performance on a range of natural language processing (NLP) tasks [1, 2]. As a consequence, we have witnessed their increasing adoption in the medical domain [3, 4]. While they achieve strong empirical performance, little is understood

---

<sup>1</sup>We refer to the clustering of the feature space according to the labels of the input datapoint.

<sup>2</sup>All code is available at [https://github.com/adelaidehsu/path\\_model\\_evaluation](https://github.com/adelaidehsu/path_model_evaluation)

about how they obtain these results or when they lead to unreliable performance. In these critical applications, interpretability of the predictions is indispensable for building trust in these models for medical personnel and patients alike. In this paper, we propose a systematic framework that provides a practical pipeline for analyzing and interpreting models fine-tuned for particular prediction tasks, focusing on important questions: model suitability for a task, feature space evolution during fine-tuning, and interpretation of fine-tuned features and failure modes. Our framework leverages a suite of analytic and visualization techniques to interpret the feature space of a fine-tuned model.

We use SUFO to comprehensively investigate the effects of pre-training data distributions for a real-world pathology report dataset, and further support our findings with a public clinical dataset, MedNLI. We evaluate five pre-trained transformer models (Appendix A.1.1) of the same size but differing in pre-training corpora (general-domain/mixed-domain/domain-specific) on our five tasks (Appendix A.1.2). In this setting, SUFO helps study the following instantiations of its general targets: (1) how much does in-domain pre-training help? (Section 3)? (2) what changes in the feature space during fine-tuning to have led to the differences in model performance (Section 4)? (3) how do we interpret the fine-tuned feature space and analyze their failure modes (Sections 5)?

We call our approach SUFO and explain below where the name SUFO stands for by making the corresponding letters bold. Each component of SUFO was chosen to yield complementary insights into each of these questions. Firstly, **S**upervised probing evaluates model features by directly using them for prediction with minimal fine-tuning and sheds light on the suitability of certain pre-trained model for a target task. We show that although pre-trained features in a domain-specific model may contain the most useful information, a domain-specific model can overfit to minority classes after fine-tuning, when class imbalance exists, while mixed-domain pre-trained models are more robust.

Secondly, **U**nsupervised similarity analysis and **F**eature Dynamics visualization study the evolution of the learned feature spaces through fine-tuning and qualitatively disambiguate these models both through their speed of convergence and the degree to which they deviate from the pre-trained initialization. We find the benefit of in-domain pre-training is manifested in faster feature disambiguation; however, the key determinants of model performance are the closeness of pre-training and target tasks and a diverse pre-training data source enabling more robust textual modeling.

Finally, through the substantial sparsification of feature spaces induced by fine-tuning, **O**utlier analysis allows for a deeper understanding of the failure modes of these models. We observe that models pre-trained with in-domain data discover a more diverse set of challenging/erroneous reports as determined by a domain expert than a general-domain model. SUFO may inform the practical use of these models by aiding in the selection of an appropriate pre-trained model, a quantitative and qualitative evaluation of these models through fine-tuning, and finally, an understanding of their failure modes for more reliable deployment.

## 2 Related Work

**Language models (LMs) performance on clinical tasks** Prior work has noted the benefits of including biomedical data in the pre-training corpora [3, 5–7], and the nuances of when and how to include such data [8]. Yet, a comprehensive analysis of the impact of these choices on transformer features remains elusive, and our work aims to provide this understanding to offer improved prescriptive recommendations for practitioners. In concurrent work, Kefeli and Tatonetti [9] released a model fine-tuned with ClinicalBERT on pathology reports for primary Gleason score extractions.<sup>3</sup> Tai et al. [10] adapts BERT to the medical domain by adding a domain-specific embedding layer and extending the vocabulary. Domain-specific models [11–14] are proposed to further mitigate the problem of distribution shifts [15] with pre-training using biomedical data only. These models have shown improved performances on biomedical benchmarks [16], and many clinical tasks spanning from medical abstraction [17], drug-target interaction identification [18], to clinical classifications [19, 20]; however, their vulnerability regarding grammatical mistakes is also discussed [21–23].

**Feature analysis in LMs** Most prior works have focused on token feature analysis in unsupervised LM encoders. Supervised probing models are widely used in such works to test features for linguistic phenomena [24–26] and syntactic structure [27]. With increased flexibility, unsupervised techniques are also proposed to investigate features in the same encoders. SV-CCA [28], a form of canonical

---

<sup>3</sup>This concurrent model isn't included in our evaluation due to time constraints before submission deadlines.

correlation analysis, is used in a cross-temporal feature analysis for learning dynamics [29], while PW-CCA [30], an improved version of SV-CCA, is used to analyze transformer features under different pre-training objectives [31]. RSA [32] is increasingly used, such as in investigating the sensitivity of features to context [33], and the correspondence of natural language features to syntax [34]. In addition to the works performed on unsupervised LMs, our work builds on a line of recent works focusing on the fine-tuning effect on BERT for NLP tasks. Peters et al. [35] discussed the choice of adaptation methods based on the performance of task-specific probing models at various layers. van Aken et al. [36] interpreted question-answering models through cluster analysis. Structural probing, RSA and layer ablations are also used in investigating the fine-tuning process of BERT [37], and correlating features of a fine-tuned BERT to fMRI voxel features [38].

Our work improves upon feature analysis since it integrates feature analyses to enable enhanced interpretability of the fine-tuned feature spaces of transformer, and provides insights into the impact of pre-training data. This integrated feature analysis pipeline SUFO allows a clearer window through which the inner workings of fine-tuned LMs become more accessible to domain experts such as clinicians. Such domain expert engagements are indispensable for building trust in LMs and ensuring their safety in medicine. See Appendix A.1 for a full description of our experimental setup.

### 3 How much does in-domain pre-training help?

In this section, we discuss realistic scenarios when in-domain pretraining <sup>4</sup> benefits, and more importantly, hinders, downstream task performances by analyzing performance of the pre-trained models under two most common forms of adaptation: fine-tuning and supervised probing.

#### 3.1 Model performance: fine-tuning

We show the fine-tuned model performance on pathology reports in Table 1. The models have generally comparable performance on Path-SG, Path-MS, and Path-SV; however, they are distinguished by their performance on Path-PG, where serious data imbalance exists. In Path-PG, BioBERT and Clinical BioBERT still obtain relatively high accuracies, > 93%, while classifying both majority *and* minority classes well (see Table A2 for per-class accuracy). The general-domain models, BERT and TNLN, having accuracies 86% and 76% on Path-PG, show inferior performance to the mixed-domain models. Yet surprisingly, PubMedBERT, as a domain-specific model, also does poorly on Path-PG by performing close to the general-domain models. Specifically, we find that while PubMedBERT does well on the majority classes, it struggles with the minority one.

To investigate whether this finding extends outside of our pathology report dataset, we evaluated the fine-tuning performance of PubMedBERT and Clinical BioBERT on MedNLI, where we simulated three scenarios of different class distributions: Balanced, Imbalanced (simulating class distribution in Path-SG), and Highly Imbalanced (simulating class distribution in Path-PG), and report the results in Table A3. In the Balanced set, PubMedBERT can outperform Clinical BioBERT. However, Clinical BioBERT outperforms PubMedBERT in the Highly Imbalanced set due to PubMedBERT’s inability to classify one of the minority groups well, while in the Imbalanced set, both yield comparable performance, corroborating our finding on the pathology reports. Hence, for the feature analyses in the following sections, we will focus on the pathology report dataset.

#### 3.2 Model performance: supervised probing

Supervised probing, where we freeze the pre-trained weights, and only train the last linear layer, is a measure of how much useful information for a downstream task is contained in the pre-trained features [36, 35, 37, 27]. We report the supervised probing performance on pathology reports in Table A4. For comparison, we provide baseline results on a randomly initialized BERT (RandomBERT). This normalization is necessary as even random features often perform well in probing methods. [39, 40]. Among all, PubMedBERT achieves the highest average score while the mixed-domain models and BERT, come second with average scores close to PubMedBERT, and TNLN obtains the lowest average score failing to even beat the baseline.

---

<sup>4</sup>In-domain pre-training includes both mixed and domain-specific pre-training, as long as biomedical data is included in the pre-training data.

Table 1: F1 test set performance over 3 runs. BioBERT and Clinical BioBERT perform the best on average, while PubMedBERT struggles when serious data imbalance present.

Models	Path-PG	Path-SG	Path-MS	Path-SV	Average
BERT	0.858 (0.16)	0.975 (0.02)	0.957 (0.01)	0.908 (0.03)	0.924
TNLR	0.763 (0.18)	0.995 (0.01)	0.963 (0.01)	0.932 (0.01)	0.913
BioBERT	0.933 (0.04)	0.991 (0.01)	0.959 (0.01)	0.915 (0.02)	0.950
Clinical BioBERT	0.959 (0.03)	0.992 (0.01)	0.964 (0.01)	0.920 (0.01)	0.959
PubMedBERT	0.770 (0.12)	0.984 (0.01)	0.970 (0.01)	0.928 (0.01)	0.913

### 3.3 Discussion on effect of in-domain pre-training data

The results in Subsections 3.1 and 3.2 demonstrate some subtle effects of in-domain pre-training data when it brings performance gain. That is, even under different degrees of class imbalance, *if* pre-training data is diverse enough to ensure robustness, the gain persists. PubMedBERT is shown to contain much useful information for our tasks in its pre-trained features, possibly due to its domain-specific pre-training; however, it suffers from instability in predicting the minority class after fine-tuning. Mixed-domain models, such as BioBERT and Clinical BioBERT, not only show good performance on supervised probing, but also perform well after fine-tuning. The benefits of their mixed-domain pre-training are two-fold: first, pre-training on biomedical datasets allows for better domain-specific features more amenable to performance improvements through fine-tuning, and second, the incorporation of general-domain corpus makes them more resistant to overfitting.

## 4 What happens during fine-tuning?

In Sec 3, we observe how fine-tuning affects PubMedBERT’s suitability for pathology classification tasks, indicating significant feature space changes. Here, we examine these changes across layers and over time. We start by using unsupervised similarity analysis to measure neural representation content similarity [41] across layers. Additionally, we explore feature dynamics through cluster analysis, examining feature disambiguation’s structure and evolution across both time and layers. Our work stands out as the first to conduct such extensive cluster analysis on text features, in contrast to previous studies that often focus solely on cross-layer or cross-temporal analysis [36, 31].

### 4.1 Unsupervised representational similarity analysis (RSA): changes in the feature space after fine-tuning

RSA is an unsupervised technique for measuring the similarity of two different feature spaces given a set of control stimuli. It was first developed in neuroscience [32], and has been increasingly used to analyze similarity between neural network activations [37, 33, 34]. To conduct RSA, a common set of  $n$  samples is used to create two sets of features from two models separately. For each feature set, a pairwise similarity matrix in  $\mathbb{R}^{n \times n}$  is calculated with a defined distance measure. The final similarity score between the two feature spaces is computed as the Pearson correlation between the flattened upper triangular sections of the two pairwise similarity matrices. In our work, we sample random reports ( $n = 1000$ ) from our dataset for each of the four tasks as the control stimuli. We extract activations of corresponding encoder layers at the classification token from the two versions, e.g. pre-trained vs. fine-tuned, of each model as the feature sets to compare, in an effort to examine the layer-wise change brought by the fine-tuning process. We use Euclidean distance as the defined distance measure to calculate the pairwise similarity matrix.

**Results** Figure A1 shows our RSA results comparing the pre-trained and fine-tuned versions of the models. In the figure, lower values imply greater change relative to the pre-trained model. We observe a few common trends across all tasks. First, the changes generally arise in the middle layers of the network, and increase in the layers closer to the loss, with little change observed in the layers closest to the input, possibly due to vanishing gradient. Second, Clinical BioBERT on average has the smallest change across layers, or retains the most pre-trained information, while TNLR undergoes the most drastic reconfiguration, suggesting Clinical BioBERT having the pre-trained data distribution more aligned to our target task which are less distorted during fine-tuning, while that of TNLR is the



most distant<sup>5</sup>. On average, BERT, BioBERT and PubMedBERT show moderate reconfiguration in the layers, which especially indicates the versatility of BERT’s feature space for its ability to match models pre-trained using in-domain data with relatively little reconfiguration.

## 4.2 Feature dynamics: cluster analysis across layer and time

We employ PCA to study feature dynamics in the models, assessing their structure and evolution during fine-tuning along two axes: layer and time. We determine whether feature disambiguation aligns with layers displaying the most change as discussed in Subsection 4.1, evaluating the practicality of this change for the tasks. Feature sets for this experiment consist of activations from corresponding encoder layers at the classification token across all 25 checkpoints.

**Results** We provide test set feature dynamics for the models in Appendix A.11, including results from Path-PG and Path-MS as representatives of tasks with varying label numbers, as we note consistent outcomes across all four tasks. When comparing feature dynamics to RSA results in Subsection 4.1, we find that changes in layers measured through RSA generally correspond to valuable information for target tasks as feature disambiguation in layers often aligns with significant drops in RSA scores across all five models. The feature dynamics of TNLN is generally the most dissimilar with the rest. For example, in Path-PG, TNLN disambiguates the minority class, 5, first starting in layer 4, and then the majority classes, 3 and 4, starting in layer 7; however, we observe the opposite behavior in the remaining BERT-based models, where they disambiguate the majority class before the minority class. We suspect this difference results from the pre-training objectives and self-attention mechanisms. Examining the feature dynamics through time, we do see models leveraging in-domain pre-training, such as BioBERT, Clinical BioBERT, and PubMedBERT, disambiguate faster than general-domain models. In Path-PG, in-domain models start to disambiguate the classes at around epoch 6, while BERT and TNLN do so around epoch 9. Overall, Clinical BioBERT requires the fewest change in layers and less training epochs to disambiguate the features well. The mixing of classes shown in PubMedBERT’s scatterplots on Path-PG, which was not observed in its train set feature dynamics, corroborates the overfitting problem that we see in its fine-tuning performance. From the result, we argue that in-domain pre-training reduces the required fine-tuning epochs, but the quality of final feature disambiguation determining a model’s performance is dependent on the closeness of pre-training and target tasks, and the model’s resistance against overfitting, exemplified by Clinical BioBERT’s fast and clear feature disambiguation.

## 5 Interpretation of the fine-tuned feature space

In this section, we perform outlier analysis on the fine-tuned final layer classification token feature spaces of the models, yielding insights into their failure modes. We find the feature spaces undergo extensive sparsification through fine-tuning (see Appendix A.9), enabling us to leverage this structure to identify outliers and solicit expert evaluation to determine the causes of this behavior. We demonstrate that different pre-trained models exhibit qualitative differences in their outlier modes and SUFO provides useful practical insight into the behavior of these models under fine-tuning.

### 5.1 Outlier extraction

To extract outliers, we construct clusters of the training set<sup>6</sup> on the two-dimensional singular subspace of the feature space. We observe a strong clustering phenomenon where most samples cluster based on their labels (see Figure 1). The main difficulties in extracting these clusters are that the one-dimensional projections onto PC1 and PC2 often exhibit significant differences in scale and distribution across the four tasks (Figure 1b) and furthermore, the cluster structure itself is also correspondingly different (Figure 1b) across tasks. To address this, we first independently extract clusters for the one-dimensional projections onto PC1 (either 2 or 3 depending on the number of labels) and PC2 (either 1 or 3). This produces intervals  $\{I_{i,1}\}_{i=1}^{m_1}$  and  $\{I_{i,2}\}_{i=1}^{m_2}$  where  $m_1, m_2 \in [3]$  for PC1 and PC2 respectively. The clusters in the top-2 singular subspace are obtained by taking the cross product of all pairs of 1-dimensional clusters to obtain  $m_1 \times m_2$  rectangles  $\{I_{i,1} \times I_{j,2}\}_{i \in [m_1], j \in [m_2]}$ .

<sup>5</sup>See Appendix A.8 for a quantitative definition of the closeness between pre-training data and target data.

<sup>6</sup>We choose the training set here to ensure there are a sufficient number of datapoints to reliably recover the PCs. This, however, limits our ability to examine the test set *generalization* of the models.

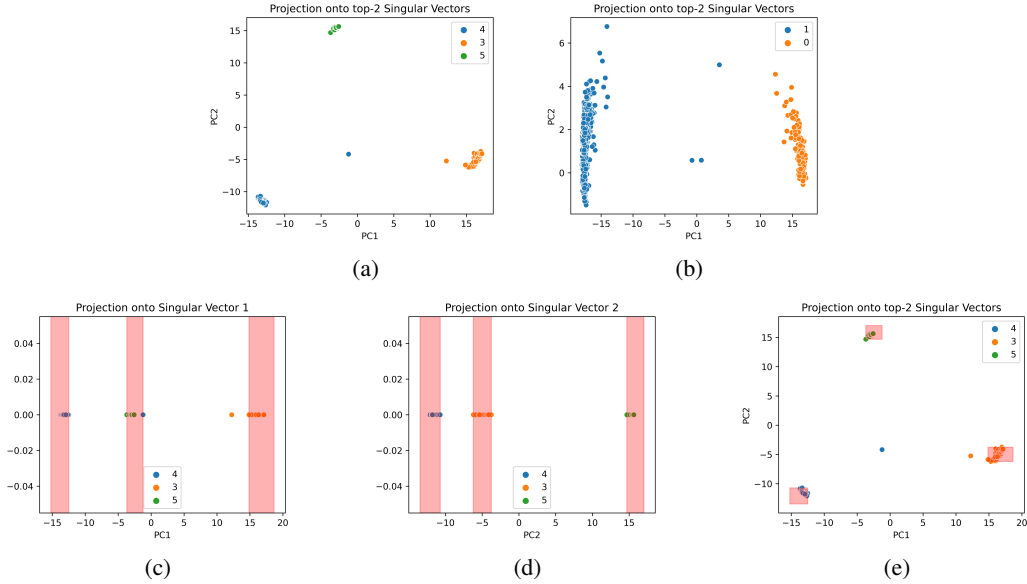


Figure 1: Illustration of clustering algorithm: fine-tuned BERT on Path-PG. (a) The projection onto the first two PCs. (b) A similar projection for Path-SV. Notice that the scales of the two PCs are drastically different and a naive clustering based on the Euclidean metric may not capture the variation in PC2. (c) The 3 clusters obtained from the projection onto PC1 with each red bar denoting the boundaries of a single cluster. (d) 3 clusters similarly obtained on PC2. (e) The final set of 3 clusters obtained by forming all possible combinations of clusters from (c) and (d) and selecting the 3 largest.

From these, the 2 or 3 (again depending on the number of labels) rectangles with the most datapoints are selected to obtain the final set of 2-dimensional clusters (represented by the red rectangles in Figure 1e). This process is illustrated in Figure 1. Finally, we extract as outliers all reports which do not fall into any of the clusters.

## 5.2 Domain Expert Evaluation

After extracting these outliers, we solicited feedback from a domain expert (a clinician in Urology) to attempt to explain their behavior. They were asked whether an outlier report would be challenging for human classification, and if so, explain why. The models were then compared on this feedback.

**Common outlier modes** We identified the following common outlier modes from our expert feedback. Here, we restrict to the reports identified as being difficult to classify by our expert, henceforth referred to as Hard Outliers: (1) Wrongly labeled reports, (2) Inconsistent reports, (3) Multiple Sources of Information, (4) Not reported or truncated report, and (5) Boundary reports. (full definition in Table A6). The main difference between models is their sensitivity to truncated/unreported (4) instances (see Hard Outliers distributions in Table A7). Clinical BioBERT and PubMedBERT identify more instances where the target label is not present than BERT, BioBERT, and TNL. Hence, the sparsified feature spaces of PubMedBERT and Clinical BioBERT allow for improved detection of missing *medical information* in the pathology reports. We believe the two models extract more comprehensive features that better model the medical data than their general counterparts. On the other hand, features extracted by PubMedBERT are less robust leading to overfitting during fine-tuning. We attribute the inferior performance of the other mixed-domain model, BioBERT, compared to Clinical BioBERT to the lack of clinical data in its pre-training corpus.

## 6 Conclusions

In this work, we developed SUFO, a systematic pipeline to shed light on the fine-tuned feature spaces of transformers for increased interpretability by domain practitioners, helping ensure trust in and

safety of LMs in critical application domains such as medicine. In our case study investigating the impact of pre-training data, we reveal the robustness of mixed-domain models under substantial class imbalance, that in-domain pre-training helps faster feature disambiguation and improved identification of missing medical information, validated by an expert evaluation. While this work represents a step toward transparent LMs in medicine, it is limited in scale and focused on clinical classification tasks. Generalizing these findings to broader clinical tasks and models requires further research.

## Acknowledgments and Disclosure of Funding

This work is partially supported by NSF DMS-grant 2015341 and NSF grant 2023505 on Collaborative Research: Foundations of Data Science Institute (FODSI). We thank Peter Potash for insightful discussions at the development stage of this work.

## References

- [1] Jacob Devlin, Ming-Wei Chang, Kenton Lee, and Kristina Toutanova. BERT: Pre-training of deep bidirectional transformers for language understanding. In *Proceedings of the 2019 Conference of the North American Chapter of the Association for Computational Linguistics: Human Language Technologies, Volume 1 (Long and Short Papers)*, pages 4171–4186, Minneapolis, Minnesota, June 2019. Association for Computational Linguistics. doi: 10.18653/v1/N19-1423. URL <https://aclanthology.org/N19-1423>.
- [2] Mike Lewis, Yinhan Liu, Naman Goyal, Marjan Ghazvininejad, Abdelrahman Mohamed, Omer Levy, Veselin Stoyanov, and Luke Zettlemoyer. BART: Denoising sequence-to-sequence pre-training for natural language generation, translation, and comprehension. In *Proceedings of the 58th Annual Meeting of the Association for Computational Linguistics*, pages 7871–7880, Online, July 2020. Association for Computational Linguistics. doi: 10.18653/v1/2020.acl-main.703. URL <https://aclanthology.org/2020.acl-main.703>.
- [3] Alexander Yalunin, Dmitriy Umerenkov, and Vladimir Kokh. Abstractive summarization of hospitalisation histories with transformer networks. *CoRR*, abs/2204.02208, 2022. doi: 10.48550/arXiv.2204.02208. URL <https://doi.org/10.48550/arXiv.2204.02208>.
- [4] Longxiang Zhang, Renato Negrinho, Arindam Ghosh, Vasudevan Jagannathan, Hamid Reza Hassanzadeh, Thomas Schaaf, and Matthew R. Gormley. Leveraging pretrained models for automatic summarization of doctor-patient conversations. In *Findings of the Association for Computational Linguistics: EMNLP 2021*, pages 3693–3712, Punta Cana, Dominican Republic, November 2021. Association for Computational Linguistics. doi: 10.18653/v1/2021.findings-emnlp.313. URL <https://aclanthology.org/2021.findings-emnlp.313>.
- [5] Colin Grambow, Longxiang Zhang, and Thomas Schaaf. In-domain pre-training improves clinical note generation from doctor-patient conversations. In *Proceedings of the First Workshop on Natural Language Generation in Healthcare*, pages 9–22, Waterville, Maine, USA and virtual meeting, July 2022. Association for Computational Linguistics. URL <https://aclanthology.org/2022.nlg4health-1.2>.
- [6] Emily Alsentzer, John Murphy, William Boag, Wei-Hung Weng, Di Jindi, Tristan Naumann, and Matthew McDermott. Publicly available clinical BERT embeddings. In *Proceedings of the 2nd Clinical Natural Language Processing Workshop*, pages 72–78, Minneapolis, Minnesota, USA, June 2019. Association for Computational Linguistics. doi: 10.18653/v1/W19-1909. URL <https://aclanthology.org/W19-1909>.
- [7] Jinhyuk Lee, Wonjin Yoon, Sungdong Kim, Donghyeon Kim, Sunkyu Kim, Chan Ho So, and Jaewoo Kang. BioBERT: a pre-trained biomedical language representation model for biomedical text mining. *Bioinformatics*, 36(4):1234–1240, 09 2019. ISSN 1367-4803. doi: 10.1093/bioinformatics/btz682. URL <https://doi.org/10.1093/bioinformatics/btz682>.
- [8] Suchin Gururangan, Ana Marasović, Swabha Swayamdipta, Kyle Lo, Iz Beltagy, Doug Downey, and Noah A. Smith. Don’t stop pretraining: Adapt language models to domains and tasks. In *Proceedings of the 58th Annual Meeting of the Association for Computational Linguistics*, pages 8342–8360, Online, July 2020. Association for Computational Linguistics. doi: 10.18653/v1/2020.acl-main.740. URL <https://aclanthology.org/2020.acl-main.740>.
- [9] Jenna Kefeli and Nicholas Tatonetti. Primarygleasonbert. <https://huggingface.co/jkefeli/PrimaryGLEasonBERT>, 2023.

- [10] Wen-Hsin Tai, H. T. Kung, and Xin Dong. exbert: Extending pre-trained models with domain-specific vocabulary under constrained training resources. In *Findings*, 2020.
- [11] Yu Gu, Robert Tinn, Hao Cheng, Michael Lucas, Naoto Usuyama, Xiaodong Liu, Tristan Naumann, Jianfeng Gao, and Hoifung Poon. Domain-specific language model pretraining for biomedical natural language processing. *ACM Trans. Comput. Healthcare*, 3(1), oct 2021. ISSN 2691-1957. doi: 10.1145/3458754. URL <https://doi.org/10.1145/3458754>.
- [12] Laila Rasmy, Yang Xiang, Ziqian Xie, Cui Tao, and Degui Zhi. Med-bert: pre-trained contextualized embeddings on large-scale structured electronic health records for disease prediction. *CoRR*, abs/2005.12833, 2020. URL <https://arxiv.org/abs/2005.12833>.
- [13] Fei Li, Yonghao Jin, Weisong Liu, Bhanu Pratap Singh Rawat, Pengshan Cai, and Hong Yu. Fine-tuning bidirectional encoder representations from transformers (bert)-based models on large-scale electronic health record notes: An empirical study. *JMIR Medical Informatics*, 7, 2019. URL <https://api.semanticscholar.org/CorpusID:202567532>.
- [14] Sungmin Aum and Seon Choe. srbert: automatic article classification model for systematic review using bert. *Systematic reviews*, 10(1):1–8, 2021.
- [15] Shang Gao, Mohammed M. Alawad, Michael T. Young, John P. Gounley, Noah Schaefferkoetter, Hong-Jun Yoon, Xiao-Cheng Wu, Eric B. Durbin, Jennifer Anne Doherty, Antoinette M. Stroup, Linda Coyle, and Georgia D. Tourassi. Limitations of transformers on clinical text classification. *IEEE Journal of Biomedical and Health Informatics*, 25:3596–3607, 2021.
- [16] Robert Tinn, Hao Cheng, Yu Gu, Naoto Usuyama, Xiaodong Liu, Tristan Naumann, Jianfeng Gao, and Hoifung Poon. Fine-tuning large neural language models for biomedical natural language processing. *Patterns*, 4(4):100729, 2023. ISSN 2666-3899. doi: <https://doi.org/10.1016/j.patter.2023.100729>. URL <https://www.sciencedirect.com/science/article/pii/S2666389923000697>.
- [17] Sam Preston, Mu-Hsin Wei, Rajesh Rao, Robert Tinn, Naoto Usuyama, Michael R. Lucas, Yu Gu, Roshanthi Weerasinghe, Soo Youl Lee, Brian D. Piening, Paul D. Tittel, Naveen Valluri, Tristan Naumann, Carlo B. Bifulco, and Hoifung Poon. Towards structuring real-world data at scale: Deep learning for extracting key oncology information from clinical text with patient-level supervision. *ArXiv*, abs/2203.10442, 2022.
- [18] Jihad Aldahdooh, Markus Vähä-Koskela, Jing Tang, and Ziaurrehman Tanoli. Using bert to identify drug-target interactions from whole pubmed. *BMC bioinformatics*, 23(1):245, 2022.
- [19] Ali S Tejani, Yee S Ng, Yin Xi, Julia R Fielding, Travis G Browning, and Jesse C Rayan. Performance of multiple pretrained bert models to automate and accelerate data annotation for large datasets. *Radiology: Artificial Intelligence*, 4(4):e220007, 2022.
- [20] J Mantas et al. The classification of short scientific texts using pretrained bert model. *Public Health and Informatics: Proceedings of MIE 2021*, 281:83, 2021.
- [21] Keno K Bressemer, Lisa C Adams, Robert A Gaudin, Daniel Tröltzsch, Bernd Hamm, Marcus R Makowski, Chan-Yong Schüle, Janis L Vahldiek, and Stefan M Niehues. Highly accurate classification of chest radiographic reports using a deep learning natural language model pre-trained on 3.8 million text reports. *Bioinformatics*, 36(21):5255–5261, 07 2020. ISSN 1367-4803. doi: 10.1093/bioinformatics/btaa668. URL <https://doi.org/10.1093/bioinformatics/btaa668>.
- [22] Phillip Richter-Pechanski, Nicolas A. Geis, Christina Kiriakou, Dominic M. Schwab, and Christoph Dieterich. Automatic extraction of 12 cardiovascular concepts from german discharge letters using pre-trained language models. *DIGITAL HEALTH*, 7, 2021. URL <https://journals.sagepub.com/doi/full/10.1177/20552076211057662>. SAGE Publications Sage UK: London, England.
- [23] Manuel Lentzen, Sumit Madan, Vanessa Lage-Rupprecht, Lisa Kühnel, Juliane Fluck, Marc Jacobs, Mirja Mittermaier, Martin Witzernath, Peter Brunecker, Martin Hofmann-Apitius, Joachim Weber, and Holger Fröhlich. Critical assessment of transformer-based AI models for German clinical notes. *JAMIA Open*, 5(4), 11 2022. ISSN 2574-2531. doi: 10.1093/jamiaopen/ooac087. URL <https://doi.org/10.1093/jamiaopen/ooac087>. ooac087.
- [24] Ian Tenney, Patrick Xia, Berlin Chen, Alex Wang, Adam Poliak, R Thomas McCoy, Najoung Kim, Benjamin Van Durme, Sam Bowman, Dipanjan Das, and Ellie Pavlick. What do you learn from context? probing for sentence structure in contextualized word representations. In *International Conference on Learning Representations*, 2019. URL <https://openreview.net/forum?id=SJzSgnRcKX>.

- [25] Nelson F. Liu, Matt Gardner, Yonatan Belinkov, Matthew E. Peters, and Noah A. Smith. Linguistic knowledge and transferability of contextual representations. In *Proceedings of the 2019 Conference of the North American Chapter of the Association for Computational Linguistics: Human Language Technologies, Volume 1 (Long and Short Papers)*, pages 1073–1094, Minneapolis, Minnesota, June 2019. Association for Computational Linguistics. doi: 10.18653/v1/N19-1112. URL <https://aclanthology.org/N19-1112>.
- [26] Matthew E. Peters, Mark Neumann, Luke Zettlemoyer, and Wen-tau Yih. Dissecting contextual word embeddings: Architecture and representation. In *Proceedings of the 2018 Conference on Empirical Methods in Natural Language Processing*, pages 1499–1509, Brussels, Belgium, October–November 2018. Association for Computational Linguistics. doi: 10.18653/v1/D18-1179. URL <https://aclanthology.org/D18-1179>.
- [27] John Hewitt and Christopher D. Manning. A structural probe for finding syntax in word representations. In *Proceedings of the 2019 Conference of the North American Chapter of the Association for Computational Linguistics: Human Language Technologies, Volume 1 (Long and Short Papers)*, pages 4129–4138, Minneapolis, Minnesota, June 2019. Association for Computational Linguistics. doi: 10.18653/v1/N19-1419. URL <https://aclanthology.org/N19-1419>.
- [28] Maithra Raghu, Justin Gilmer, Jason Yosinski, and Jascha Sohl-Dickstein. Svcca: Singular vector canonical correlation analysis for deep learning dynamics and interpretability. In *Proceedings of the 31st International Conference on Neural Information Processing Systems, NIPS’17*, page 6078–6087, Red Hook, NY, USA, 2017. Curran Associates Inc. ISBN 9781510860964.
- [29] Naomi Saphra and Adam Lopez. Understanding learning dynamics of language models with SVCCA. In *Proceedings of the 2019 Conference of the North American Chapter of the Association for Computational Linguistics: Human Language Technologies, Volume 1 (Long and Short Papers)*, pages 3257–3267, Minneapolis, Minnesota, June 2019. Association for Computational Linguistics. doi: 10.18653/v1/N19-1329. URL <https://aclanthology.org/N19-1329>.
- [30] Ari S. Morcos, Maithra Raghu, and Samy Bengio. Insights on representational similarity in neural networks with canonical correlation. In *Proceedings of the 32nd International Conference on Neural Information Processing Systems, NIPS’18*, page 5732–5741, Red Hook, NY, USA, 2018. Curran Associates Inc.
- [31] Elena Voita, Rico Sennrich, and Ivan Titov. The bottom-up evolution of representations in the transformer: A study with machine translation and language modeling objectives. In *Proceedings of the 2019 Conference on Empirical Methods in Natural Language Processing and the 9th International Joint Conference on Natural Language Processing (EMNLP-IJCNLP)*, pages 4396–4406, Hong Kong, China, November 2019. Association for Computational Linguistics. doi: 10.18653/v1/D19-1448. URL <https://aclanthology.org/D19-1448>.
- [32] Nikolaus Kriegeskorte, Marieke Mur, and Peter Bandettini. Representational similarity analysis - connecting the branches of systems neuroscience. *Frontiers in Systems Neuroscience*, 2, 2008. ISSN 1662-5137. doi: 10.3389/neuro.06.004.2008. URL <https://www.frontiersin.org/articles/10.3389/neuro.06.004.2008>.
- [33] Samira Abnar, Lisa Beinborn, Rochelle Choenni, and Willem Zuidema. Blackbox meets blackbox: Representational similarity & stability analysis of neural language models and brains. In *Proceedings of the 2019 ACL Workshop BlackboxNLP: Analyzing and Interpreting Neural Networks for NLP*, pages 191–203, Florence, Italy, August 2019. Association for Computational Linguistics. doi: 10.18653/v1/W19-4820. URL <https://aclanthology.org/W19-4820>.
- [34] Grzegorz Chrupała and Afra Alishahi. Correlating neural and symbolic representations of language. In *Proceedings of the 57th Annual Meeting of the Association for Computational Linguistics*, pages 2952–2962, Florence, Italy, July 2019. Association for Computational Linguistics. doi: 10.18653/v1/P19-1283. URL <https://aclanthology.org/P19-1283>.
- [35] Matthew E. Peters, Sebastian Ruder, and Noah A. Smith. To tune or not to tune? adapting pretrained representations to diverse tasks. In Isabelle Augenstein, Spandana Gella, Sebastian Ruder, Katharina Kann, Burcu Can, Johannes Welbl, Alexis Conneau, Xiang Ren, and Marek Rei, editors, *Proceedings of the 4th Workshop on Representation Learning for NLP, Repl4NLP@ACL 2019, Florence, Italy, August 2, 2019*, pages 7–14. Association for Computational Linguistics, 2019. doi: 10.18653/v1/w19-4302. URL <https://doi.org/10.18653/v1/w19-4302>.
- [36] Betty van Aken, Benjamin Winter, Alexander Löser, and Felix A. Gers. How does bert answer questions? a layer-wise analysis of transformer representations. In *Proceedings of the 28th ACM International Conference on Information and Knowledge Management, CIKM ’19*, page 1823–1832, New York, NY, USA, 2019. Association for Computing Machinery. ISBN 9781450369763. doi: 10.1145/3357384.3358028. URL <https://doi.org/10.1145/3357384.3358028>.

- [37] Amil Merchant, Elahe Rahimtoroghi, Ellie Pavlick, and Ian Tenney. What happens to BERT embeddings during fine-tuning? In *Proceedings of the Third BlackboxNLP Workshop on Analyzing and Interpreting Neural Networks for NLP*, pages 33–44, Online, November 2020. Association for Computational Linguistics. doi: 10.18653/v1/2020.blackboxnlp-1.4. URL <https://aclanthology.org/2020.blackboxnlp-1.4>.
- [38] Jon Gauthier and R. Levy. Linking artificial and human neural representations of language. In *Conference on Empirical Methods in Natural Language Processing*, 2019.
- [39] Kelly Zhang and Samuel Bowman. Language modeling teaches you more than translation does: Lessons learned through auxiliary syntactic task analysis. In *Proceedings of the 2018 EMNLP Workshop BlackboxNLP: Analyzing and Interpreting Neural Networks for NLP*, pages 359–361, Brussels, Belgium, November 2018. Association for Computational Linguistics. doi: 10.18653/v1/W18-5448. URL <https://aclanthology.org/W18-5448>.
- [40] John Hewitt and Percy Liang. Designing and interpreting probes with control tasks. *ArXiv*, abs/1909.03368, 2019.
- [41] Aarre Laakso and G. Cottrell. Content and cluster analysis: Assessing representational similarity in neural systems. *Philosophical Psychology*, 13:47 – 76, 2000.
- [42] Ashish Vaswani, Noam Shazeer, Niki Parmar, Jakob Uszkoreit, Llion Jones, Aidan N Gomez, Łukasz Kaiser, and Illia Polosukhin. Attention is all you need. In I. Guyon, U. Von Luxburg, S. Bengio, H. Wallach, R. Fergus, S. Vishwanathan, and R. Garnett, editors, *Advances in Neural Information Processing Systems*, volume 30. Curran Associates, Inc., 2017. URL [https://proceedings.neurips.cc/paper\\_files/paper/2017/file/3f5ee243547dee91fbd053c1c4a845aa-Paper.pdf](https://proceedings.neurips.cc/paper_files/paper/2017/file/3f5ee243547dee91fbd053c1c4a845aa-Paper.pdf).
- [43] Yukun Zhu, Ryan Kiros, Rich Zemel, Ruslan Salakhutdinov, Raquel Urtasun, Antonio Torralba, and Sanja Fidler. Aligning books and movies: Towards story-like visual explanations by watching movies and reading books. In *The IEEE International Conference on Computer Vision (ICCV)*, December 2015.
- [44] Yonghui Wu, Mike Schuster, Zhifeng Chen, Quoc V. Le, Mohammad Norouzi, Wolfgang Macherey, Maxim Krikun, Yuan Cao, Qin Gao, Klaus Macherey, Jeff Klingner, Apurva Shah, Melvin Johnson, Xiaobing Liu, Lukasz Kaiser, Stephan Gouws, Yoshikiyo Kato, Taku Kudo, Hideto Kazawa, Keith Stevens, George Kurian, Nishant Patil, Wei Wang, Cliff Young, Jason Smith, Jason Riesa, Alex Rudnick, Oriol Vinyals, Greg Corrado, Macduff Hughes, and Jeffrey Dean. Google’s neural machine translation system: Bridging the gap between human and machine translation. *CoRR*, abs/1609.08144, 2016. URL <http://arxiv.org/abs/1609.08144>.
- [45] Hangbo Bao, Li Dong, Furu Wei, Wenhui Wang, Nan Yang, Xiaodong Liu, Yu Wang, Songhao Piao, Jianfeng Gao, Ming Zhou, and Hsiao-Wuen Hon. Unilmv2: Pseudo-masked language models for unified language model pre-training. *CoRR*, abs/2002.12804, 2020. URL <https://arxiv.org/abs/2002.12804>.
- [46] Yinhan Liu, Myle Ott, Naman Goyal, Jingfei Du, Mandar Joshi, Danqi Chen, Omer Levy, Mike Lewis, Luke Zettlemoyer, and Veselin Stoyanov. Roberta: A robustly optimized bert pretraining approach. *ArXiv*, abs/1907.11692, 2019.
- [47] Trieu H. Trinh and Quoc V. Le. A simple method for commonsense reasoning. *ArXiv*, abs/1806.02847, 2018.
- [48] Anobel Y Odisho, Briton Park, Nicholas Altieri, John DeNero, Matthew R Cooperberg, Peter R Carroll, and Bin Yu. Natural language processing systems for pathology parsing in limited data environments with uncertainty estimation. *JAMIA Open*, 3(3):431–438, 10 2020. ISSN 2574-2531. doi: 10.1093/jamiaopen/ooaa029. URL <https://doi.org/10.1093/jamiaopen/ooaa029>.
- [49] Alexey Romanov and Chaitanya Shivade. Lessons from natural language inference in the clinical domain. URL <http://arxiv.org/abs/1808.06752>.

## A Appendix

### A.1 Experimental Setup

#### A.1.1 Pre-trained Models

We evaluate five 110M-sized<sup>7</sup> encoder-based<sup>8</sup> transformer [42] models commonly used in clinical classifications. Here we describe the models, with an emphasis on their differences in pre-training objectives and categories of pre-training corpora.

**General-domain: BERT and TNL** The popular BERT [1] architecture is based on bidirectional transformer encoder [42]. BERT is pre-trained on masked language-modeling (MLM) and next sentence prediction tasks, with a general-domain corpus (3.3B words) from BooksCorpus [43] and English Wikipedia. We use BERT<sub>BASE</sub> with 12 layers and 12 attention heads, and the uncased WordPiece [44] tokenization since prior work [11] has established that case does not have a significant impact on biomedical downstream tasks. The Turing Natural Language Representation (TNLR) model [45] we use has the same architecture and vocabulary as BERT. They do differ, however, in their pre-training objectives, self-attention mechanism, and data as TNLR is trained using constrained self-attention with a pseudo-masked language modeling (PMLM) [45] task on a more diverse general-domain corpus (160GB) that additionally includes OpenWebText<sup>9</sup>, CC-News [46], and Stories [47].

**Mixed-domain: BioBERT and Clinical BioBERT** BioBERT [7] and Clinical BioBERT [6] are categorized as mixed-domain pre-trained models because they are pre-trained with biomedical data on top of a general-domain corpus. The version we use is obtained via continual pre-training from BERT by training on PubMed abstracts (4.5B) for additional steps. Clinical BioBERT is the result of continual pre-training from BioBERT by training additionally on MIMIC-III clinical notes (0.5B) to be more tailored for clinical tasks. The two models share the same vocabulary and architecture as BERT.

**Domain-specific: PubMedBERT** PubMedBERT [11] was proposed to mitigate the shortcomings in BERT’s vocabulary as it cannot represent biomedical terms in full, which was found to possibly hinder the performance of general-domain and mixed-domain models on downstream biomedical tasks [16, 10, 15]. Hence, this model is trained from scratch using PubMed abstracts (3.1B) only, resulting in a more specialized vocabulary for biomedical tasks. We use the uncased version of PubMedBERT with the same architecture as BERT.

**Remark on differences in pre-training objectives and data** The pre-training objectives and data sizes are similar for all the BERT-based models and we do not expect these differences to impact our findings. While TNLR has a different objective and self-attention mechanism which could confound our analysis, we find that the quantitative and qualitative behavior observed in its analysis in relation to the mixed and domain-specific models are similar to BERT, the other general-domain model. Thus, we believe that our conclusions are applicable to TNLR despite these differences.

#### A.1.2 Fine-tuning Data

**Prostate Cancer Pathology Reports** We collected a corpus of 2907 structured pathology reports with data elements extracted from a set of free-text reports following a previously proposed preprocessing pipeline [48]. The corpus includes pathology reports for patients that had undergone radical prostatectomy for prostate cancer at the University of California, San Francisco (UCSF) from 2001 to 2018. This study was conducted under an institutional review board (IRB) approval. The reports contain an average of 471 tokens. For each document, we focus on the following 4 pathologic data elements: primary Gleason grade (Path-PG), secondary Gleason grade (Path-SG), margin status for tumor (Path-MS), and seminal vesicle invasion (Path-SV), and formed 4 classification tasks correspondingly. (Detailed description in Appendix A.2) For Path-PG and Path-SG, there are 5 labels

<sup>7</sup>Models exhibit only small changes in vocabulary sizes (28996-30522) and the 110M parameter counts include the sizes of the word embeddings.

<sup>8</sup>We focus our discussion on strictly encoder-based transformers by not considering transformers in other architectures (i.e. decoder-only, encoder-decoder) to avoid introducing extra confounding factors.

<sup>9</sup>skyllion007.github.io/OpenWebTextCorpus

available: [null, 2, 3, 4, 5], with null denoting an undecided Gleason score, often due to previous treatment effects. We exclude reports with null and 2 Gleason scores under a doctor’s suggestion as the two labels account for only 1.3% and 0.07% of the corpus, and are rarely graded in practice.<sup>10</sup> After the removal, the distribution of labels 3, 4, and 5 in Path-PG is 67%, 30%, and 3% respectively, while in Path-SG it is 39%, 53%, and 8%. Both Path-MS and Path-SV are binary classification tasks, with only two labels: [positive, negative]. The distribution of positive and negative in Path-MS is 26% and 74%, while in Path-SV is 13% and 87%. Our pathology reports dataset is not publicly available due to the protected patient information in the dataset; however, we provide a few anonymized report samples in Appendix A.3 as illustration.

**MedNLI** To support the generalizability of our conclusions, we additionally report the fine-tuning results of the models on a publicly available clinical dataset, MedNLI [49]. The objective of MedNLI is to determine if a given clinical hypothesis can be inferred from a given premise, and the dataset is labelled with three classes [contradiction, entailment, neutral]. We (non-uniformly) sample subsets of 6990 samples from MedNLI which reflect the different class distributions observed in the pathology report extraction tasks.

### A.1.3 Fine-tuning

We fine-tune the models to perform single-label classification for all tasks. We add a linear layer followed by a softmax function to the model output on the classification token. The datasets are divided into 71% training, 18% validation, and 11% test, with label distribution in each set resembling the distribution in the full datasets. Best model checkpoints are selected based on validation set performances, and are used in all experiments. For pathology reports, we evaluate the models against macro F1 as each class accounts for equal importance, while we report accuracy for MedNLI. We set the encoder sequence length to 512 tokens for pathology reports, and 256 tokens for MedNLI, which allows us to encode the full length of the majority of the datasets. Note that random weighted sampling was implemented for all tasks during fine-tuning to tackle the data imbalance.

**Prostate Cancer Pathology Reports** We use consistent fine-tuning hyperparameters for all models and all the four tasks, as we observe the validation set performance is not very sensitive to hyperparameter selection (less than 1% F1 performance change). We use an AdamW optimizer with a  $7.6 \times 10^{-6}$  learning rate, 0.01 weight decay, and a  $1 \times 10^{-8}$  epsilon. We also adopt a linear learning rate schedule with a 0.2 warm-up ratio. We fine-tune for a maximum of 25 epochs with a batch size of 8 and evaluate every 50 steps on the validation set. Each model is fine-tuned on a single NVIDIA Tesla K80 GPU, and average fine-tuning time is around 3 hours.

**MedNLI** We use consistent fine-tuning hyperparameters for all models, as we observe the validation set performance is not very sensitive to hyperparameter selection (less than 1% accuracy change). We use an AdamW optimizer with a per-layer learning rate decay schedule ( $1 \times 10^{-4}$  as the starting learning rate, and 0.8 as the decay factor), 0 weight decay,  $1 \times 10^{-6}$  epsilon, and a 0.1 warm-up ratio. We fine-tune for a maximum of 10 epochs with a batch size of 32 and evaluate every epoch on the validation set. Each model is fine-tuned on a single NVIDIA GeForce GTX TITAN X GPU, and the fine-tuning time on average is less than 1 hours.

---

<sup>10</sup>Previously we tried to include Gleason scores null and 2 in the fine-tuning, but found none of the models could classify any of the two classes well due to their extremely small sample sizes. It didn’t seem reasonable to discuss the models’ performance on these two classes given that they couldn’t even learn well.



## A.2 Description of extracted pathologic data elements

Table A1: Description of the 4 extracted pathologic data elements.

Data elements	Description
Primary Gleason grade	A whole number from 1 to 5 representing the primary score given to a specimen based on the Gleason grading system to measure tumor aggressiveness.
Secondary Gleason grade	A whole number from 1 to 5 representing the secondary score given to a specimen based on the Gleason grading system to measure tumor aggressiveness.
Margin status for tumor	To evaluate surgical margins, the entire prostate surface is inked after removal. The surgical margins are designated as "negative" if the tumor is not present at the inked margin, and "positive" if tumor is present.
Seminal vesicle invasion	Invasion of tumor into the seminal vesicle. It is marked as "negative" if no invasion is present in the seminal vesicle, and "positive" if invasion is present.

## A.3 Anonymized pathology report samples

- synoptic comment for prostate tumors " 1. type of tumor : adenocarcinoma small acinar type. " 2. location of tumor : both lobes. 3. estimated volume of tumor : 3. 5 ml. 4. gleason score : 4 + 3 = 7. 5. estimated volume > gleason pattern 3 : 2 ml. 6. involvement of capsule : present ( e. g. slide b6 ). 7. extraprostatic extension : not identified. 8. status of excision margins for tumor : negative. status of excision margins for benign prostate glands : positive ( e. g. slide b4 ). 9. involvement of seminal vesicle : not identified. 10. perineural infiltration : present ( e. g. slide b11 ). " 11. prostatic intraepithelial neoplasia ( pin ) : present high - grade ( e. g " slide b4 ). 12. ajcc / uicc stage : pt2cnxmx ; stage ii if no metastases are identified. 13. additional comments : none. final diagnosis : " a. prostate left apical margin : benign prostatic tissue. " " b. prostate and seminal vesicles resection : prostatic adenocarcinoma " gleason score 4 + 3 = 7 ; see comment.
- synoptic comment for prostate tumors - type of tumor : small acinar adenocarcinoma. - location of tumor : - right anterior midgland : slides b3 - b5. - right posterior midgland : slides b6 - b8. - left anterior midgland : slides b12 - b14. - left posterior midgland : slides b9 - b11. - left and central bladder bases : slides b16 - b17 - estimated volume of tumor : 10 cm3. " - gleason score : 7 ; primary pattern 3 secondary pattern 4. " - estimated volume > gleason pattern 3 : 40 %. " - involvement of capsule : tumor invades capsule but does not extend beyond " " capsule ( slides b5 b8 b18 ). " - extraprostatic extension : none. - margin status for tumor : negative. - margin status for benign prostate glands : negative. - high - grade prostatic intraepithelial neoplasia ( hgpin ) : present ; extensive. - tumor involvement of seminal vesicle : none. - perineural infiltration : present. - lymph node status : none submitted. - ajcc / uicc stage : pt2cnx. final diagnosis : " a. prostate left base biopsy : fibromuscular tissue no tumor. " " b. prostate radical prostatectomy : " " 1. prostatic adenocarcinoma gleason grade 3 + 4 score = 7 involving "

" bilateral prostate negative margins ; see comment. 2. " seminal vesicles with no significant pathologic abnormality.

#### A.4 Per-class accuracy on Path-PG and Path-SG

Table A2: Per-class accuracy of the five models on Path-PG and Path-SG, averaged across three runs (all stds are < 5% so we omit it to save spaces). PubMedBERT performs poorly when classifying the minority class 5 in the highly imbalanced Path-PG dataset, while it obtains descent performance across all classes in the slightly more balanced Path-SG dataset.

Models \ Labels	Path-PG			Path-SG		
	3	4	5	3	4	5
BERT	0.99	0.94	1.00	0.98	0.98	0.97
TNLR	0.97	0.87	1.00	0.99	0.99	0.99
BioBERT	0.99	0.97	0.94	0.99	0.99	0.99
Clinical BioBERT	0.99	0.98	1.00	0.99	0.99	0.98
PubMedBERT	0.99	0.92	<b>0.67</b>	0.98	0.99	0.97

#### A.5 Fine-tuning results on MedNLI

Table A3: Per-class accuracy and overall accuracy of PubMedBERT and Clinical BioBERT on MedNLI across three runs, where three scenarios are evaluated: Balanced ('C':'E':'N'=34%:33%:33%), Imbalanced ('C':'E':'N'=39%:53%:8%), and Highly Imbalanced ('C':'E':'N'=67%:30%:3%).

Labels \ Models	Balanced		Imbalanced		Highly Imbalanced	
	PubMedBERT	Clinical BioBERT	PubMedBERT	Clinical BioBERT	PubMedBERT	Clinical BioBERT
Contradiction ('C')	0.88 (0.03)	0.76 (0.03)	0.76 (0.03)	0.70 (0.02)	0.80 (0.01)	0.79 (0.03)
Entailment ('E')	0.75 (0.02)	0.71 (0.02)	0.71 (0.03)	0.70 (0.02)	0.34 (0.02)	0.62 (0.05)
Neutral ('N')	0.77 (0.05)	0.72 (0.01)	0.33 (0.16)	0.32 (0.01)	0.04 (0.03)	0.04 (0.02)
Accuracy	0.83 (0.01)	0.73 (0.01)	0.70 (0.02)	0.71 (0.01)	0.71 (0.01)	0.76 (0.03)

#### A.6 Supervised probing results on pathology reports

Table A4: F1 test set performance under supervised probing over 3 runs. PubMedBERT performs the best, showing its pre-trained feature contains the most useful information for pathology reports.

Models	Path-PG	Path-SG	Path-MS	Path-SV	Average
BERT	0.371 (0.04)	0.345 (0.05)	0.678 (0.03)	0.578 (0.02)	0.493
TNLR	0.271 (0.01)	0.267 (0.06)	0.494 (0.03)	0.481 (0.01)	0.378
BioBERT	0.340 (0.04)	0.327 (0.04)	0.666 (0.03)	0.574 (0.02)	0.477
Clinical BioBERT	0.341 (0.03)	0.336 (0.04)	0.689 (0.02)	0.581 (0.01)	0.487
PubMedBERT	0.387 (0.01)	0.327 (0.03)	0.687 (0.02)	0.575 (0.01)	0.494
Random-BERT	0.339 (0.06)	0.260 (0.09)	0.529 (0.05)	0.555 (0.05)	0.421

## A.7 RSA results on pathology reports

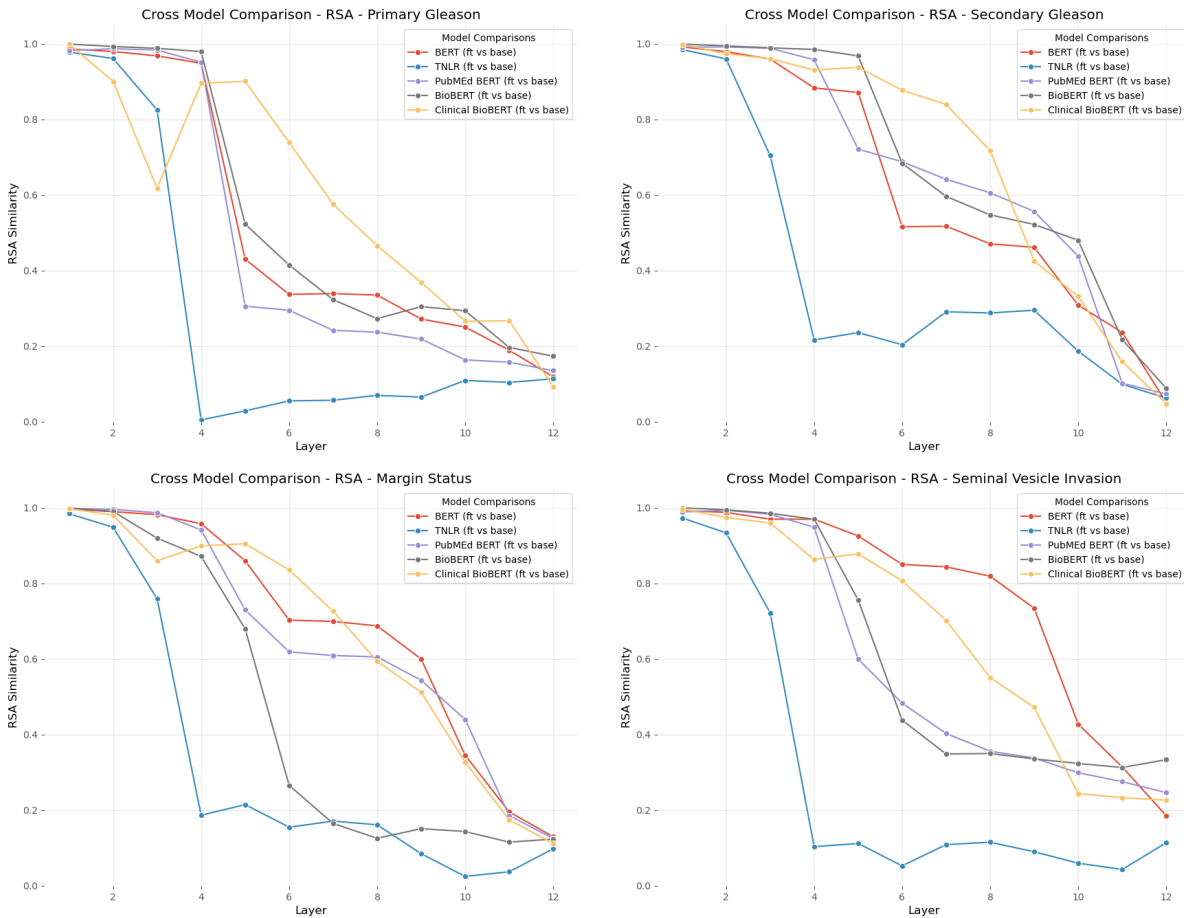


Figure A1: Layer-wise RSA comparing the pre-trained and fine-tuned versions of the models across four pathology classification tasks.

## A.8 Quantifying the closeness between pre-training data and target data

We use perplexity of pre-trained models on target tasks to define the closeness between pre-training data and target data. The lower the perplexity means the closer the two data distributions should be.

Table A5: Perplexity of the five models on pathology reports.

	BERT	TNLr	BioBERT	Clinical BioBERT	PubMedBERT
Perplexity	1.111	1.115	1.113	1.110	1.103

## A.9 The structure of the fine-tuned feature space

We analyze principle components (PCs) of features in the final layer classification token of the fine-tuned models. These features are important as they are used directly for prediction, and often contribute the most to performance in ablation studies [37, 36].

**High sparsity** We show that the fine-tuned last layer classification token feature space is highly sparsified. We observe that, for every model across the four pathology tasks, the first two PCs explain

on average 95% of the variance in the dataset (Figure A2). To understand how the PCs contribute to model performance, we conduct a PC probing experiment (Figure A3). In the experiment, we measure model performance on reconstructed rank- $k$  feature space by projecting onto the bottom  $k$  PCs, with  $k$  varying between 1 and 768. In particular,  $k = 768$  corresponds to the full-feature space. In the PC probing result, we see the first 2 PCs contribute significantly to model performance from the surge in the performance after adding them back in at  $k = 767$  and  $k = 768$ .

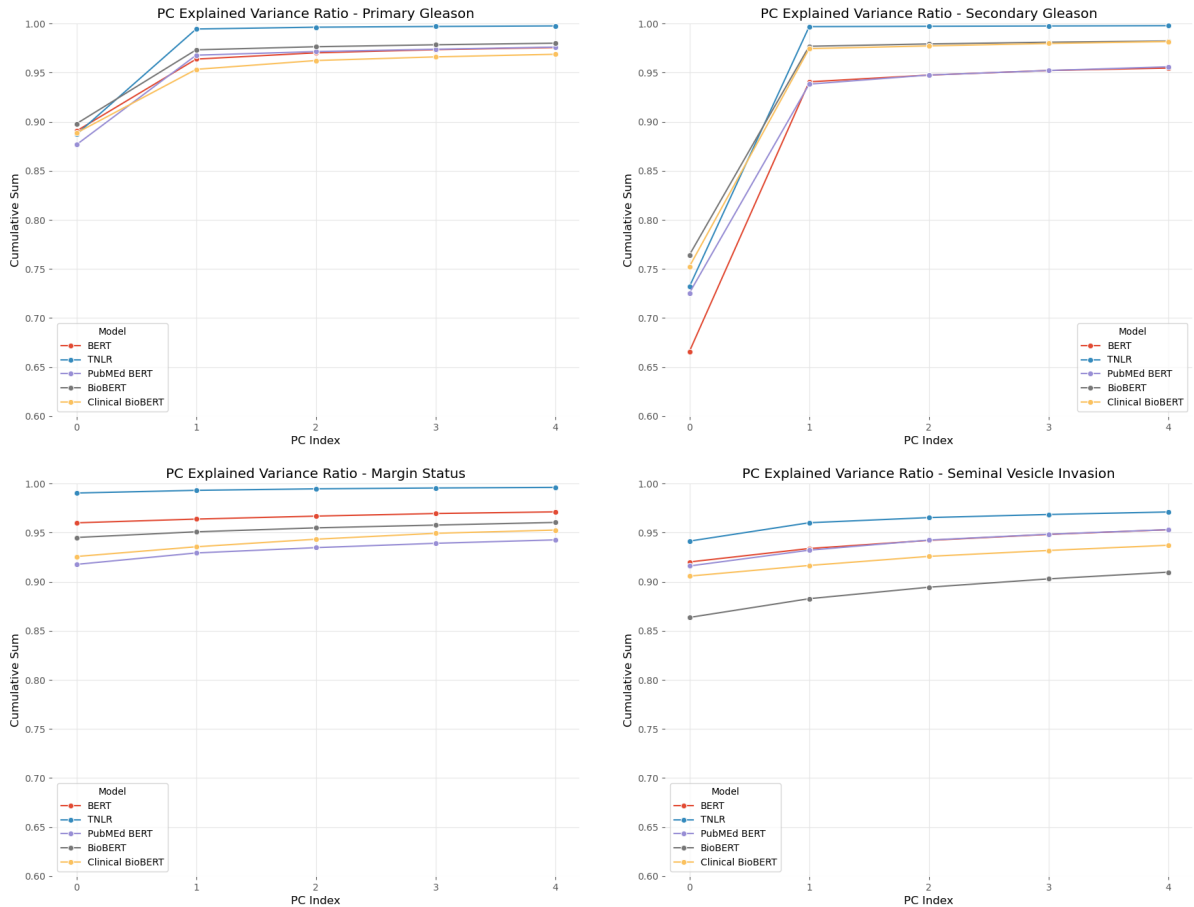


Figure A2: The first two PCs in the fine-tuned last layer classification token feature spaces of all the models explain on average 95% of the dataset variance across the 4 tasks.

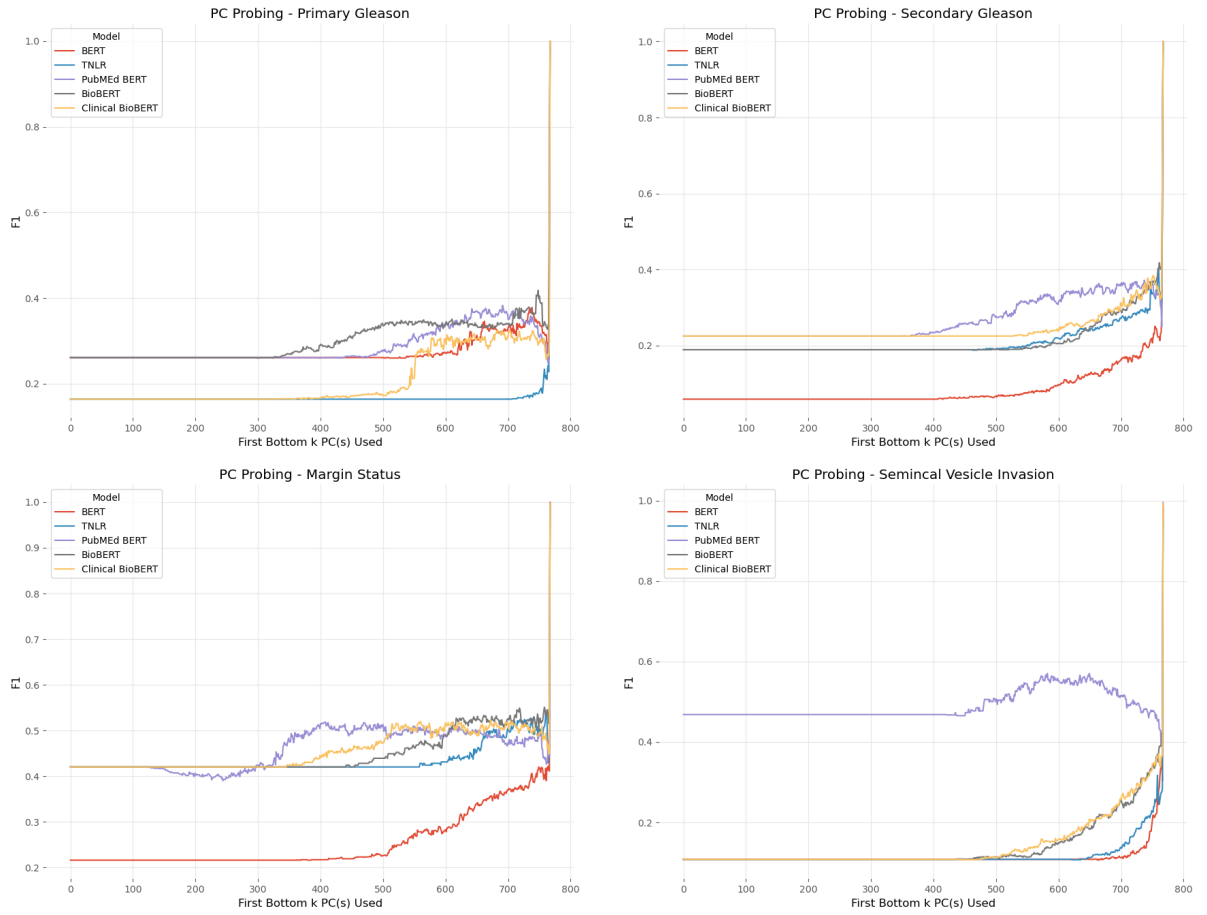


Figure A3: Filling back in the first two PCs, at the last two steps,  $k = 767$  and  $k = 768$ , yields significant model performance gain.

## A.10 Auxiliary Material for Section 5.2

Table A6: Description of categories of hard outliers

Outlier Category ID	Category Name	Category Description
1	Wrongly labeled report	These are reports for which the provided annotation is incorrect. For example, a report with null Gleason score corresponding to a scenario where a Gleason score cannot be assigned is wrongly included with another label.
2	Inconsistent report	For these reports, there exists inconsistent declarations of the target attribute (say, Primary Gleason score) in two different parts of the report.
3	Multiple Sources of Information	These reports contain multiple sources of information which are composed to produce one final label. One such instance of such an outlier (for the Secondary Gleason label) contained scores from five tumor nodules which were then combined to give one final composite score. A classifier must learn to distinguish the true final score from those that were used to obtain it.
4	Not reported or truncated report	These are reports for which the target attribute is either not reported or the report is truncated before entry into the database.
5	Boundary reports	These reports feature scenarios where the target attribute is hard to determine precisely or requires some interpretation of the provided information. For instance, one such report presents a Gleason score with a combined value of 7 with the other information in the report requiring the classifier to deduce that the Gleason score is $3 + 4$ .

Table A7: A distribution of Hard Outliers for each model categorized according to the 5 outlier types.

Outlier Type	BERT	BioBERT	Clinical BioBERT	PubMedBERT	TNLR
1	0	0	1	1	1
2	0	1	0	1	2
3	2	0	1	1	1
4	0	1	3	5	1
5	4	0	3	3	2
Total	6	2	8	11	7

## A.11 Feature dynamics

Here we present comprehensive sets of feature scatterplots along layers 1 to layer 12 (top-down) and selected epochs in the order of 1, 2, 3, 4, 5, 6, 7, 8, 9, 10, 15, 20, 25 (left-right) of the 5 models, as we observe the models typically show the most rapid performance gain from epoch 1 to 10, and marginal increase afterwards. We include the plots from Path-PG and Path-MS, as representatives of tasks having different number of labels to save space, but note that we observe similar trend in the results of all the 4 tasks

## A.11.1 Path-PG

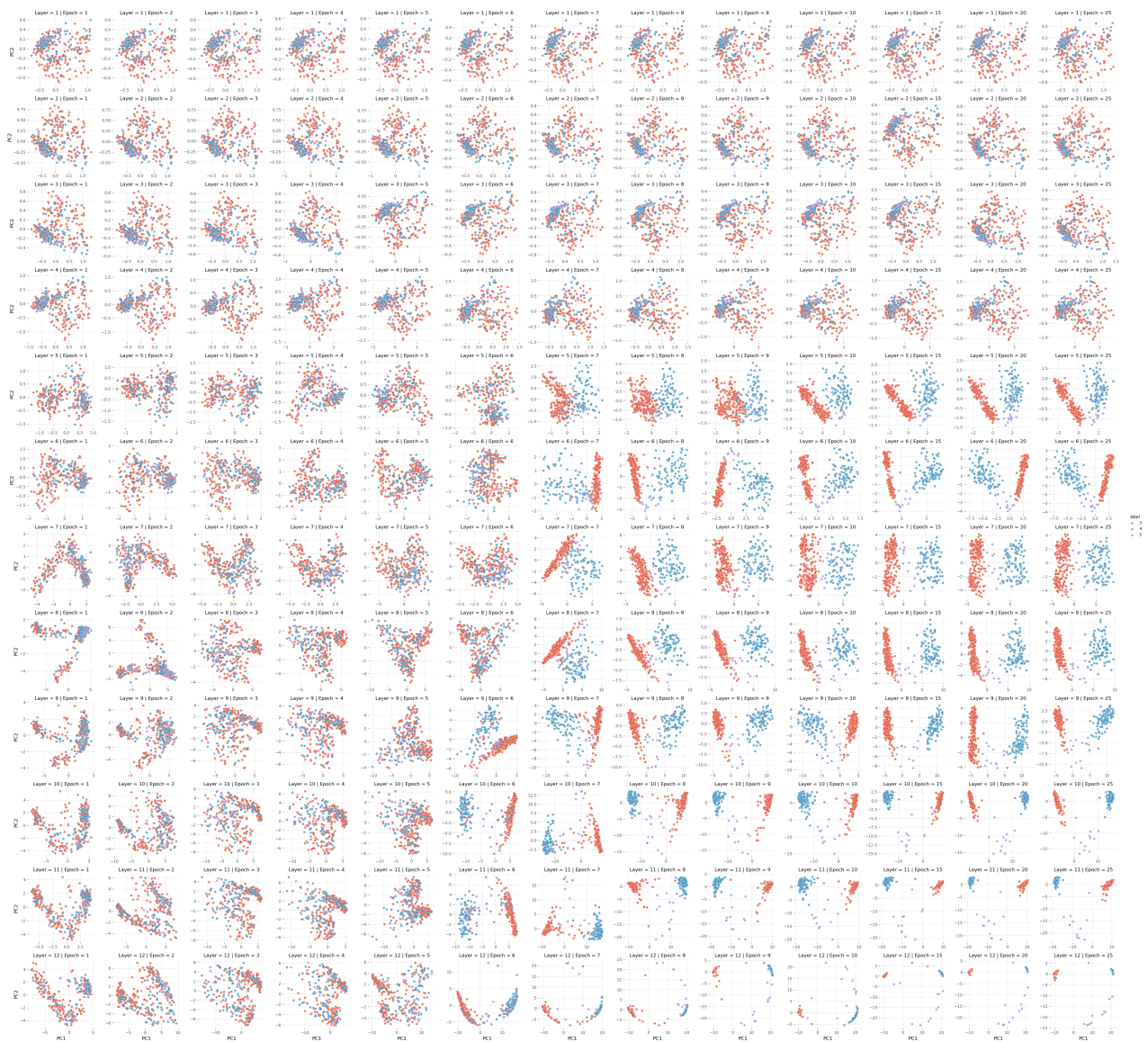


Figure A4: Path-PG: BERT

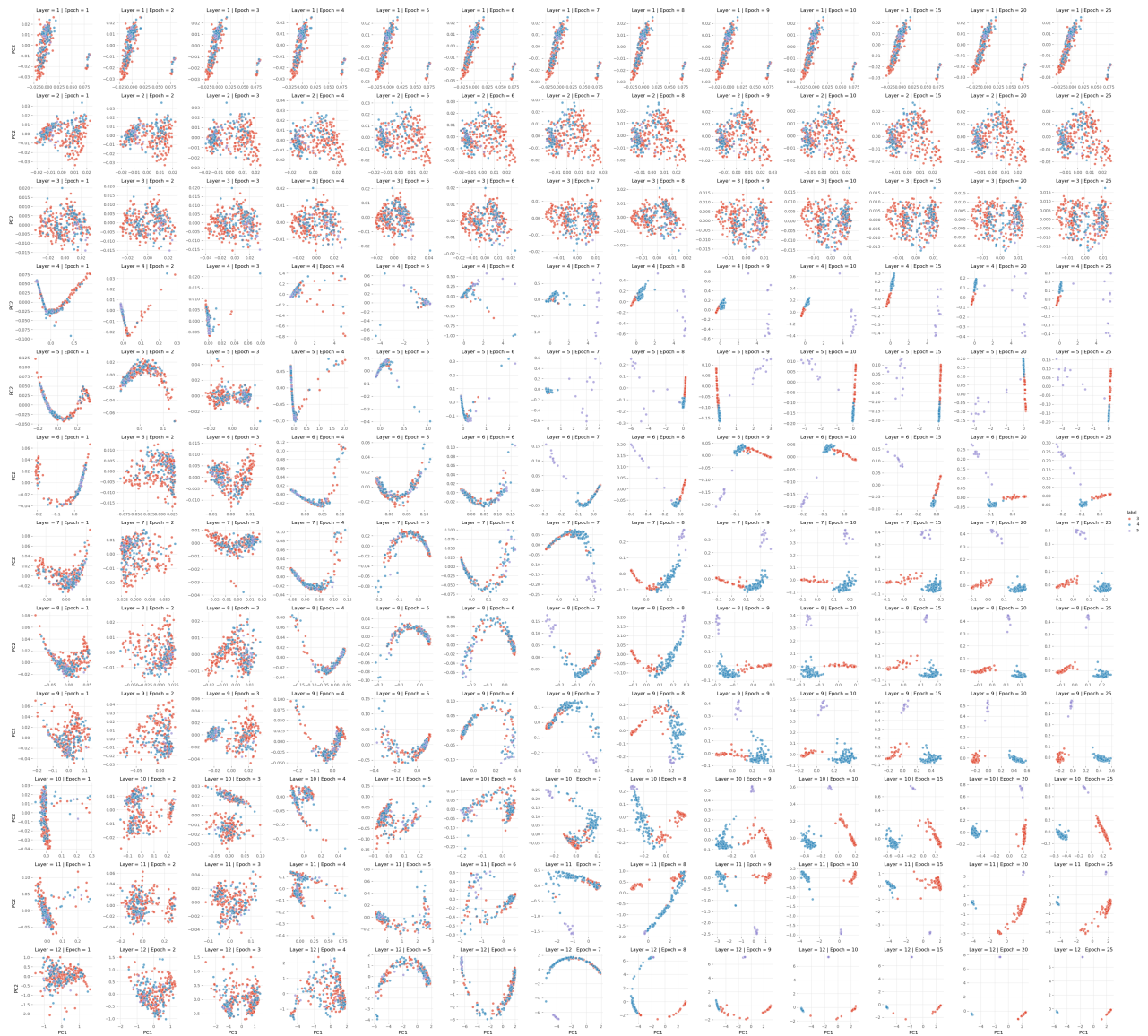


Figure A5: Path-PG: TNL



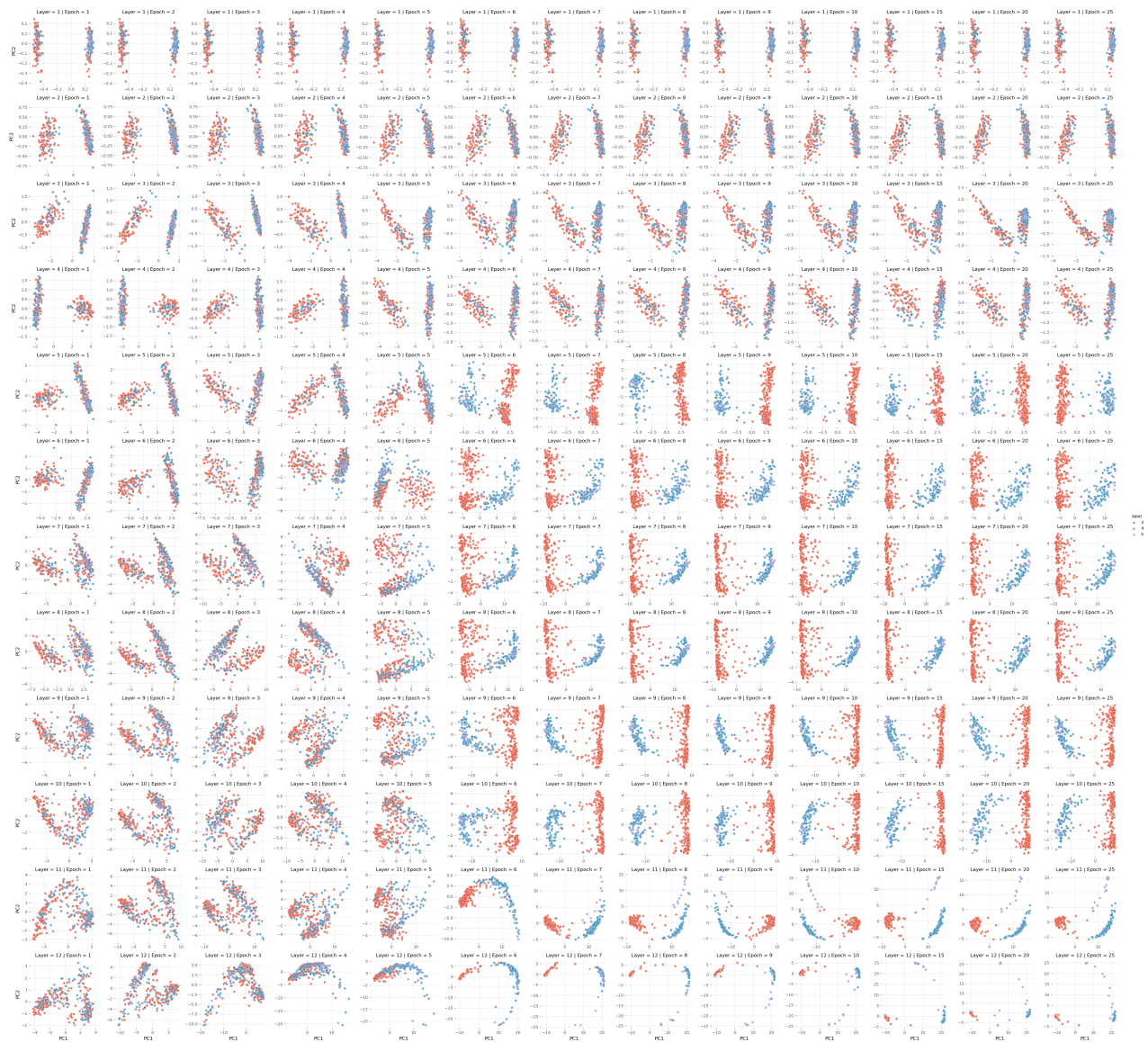


Figure A6: Path-PG: BioBERT



Figure A7: Path-PG: Clinical BioBERT



Figure A8: Path-PG: PubMedBERT



## A.11.2 Path-MS

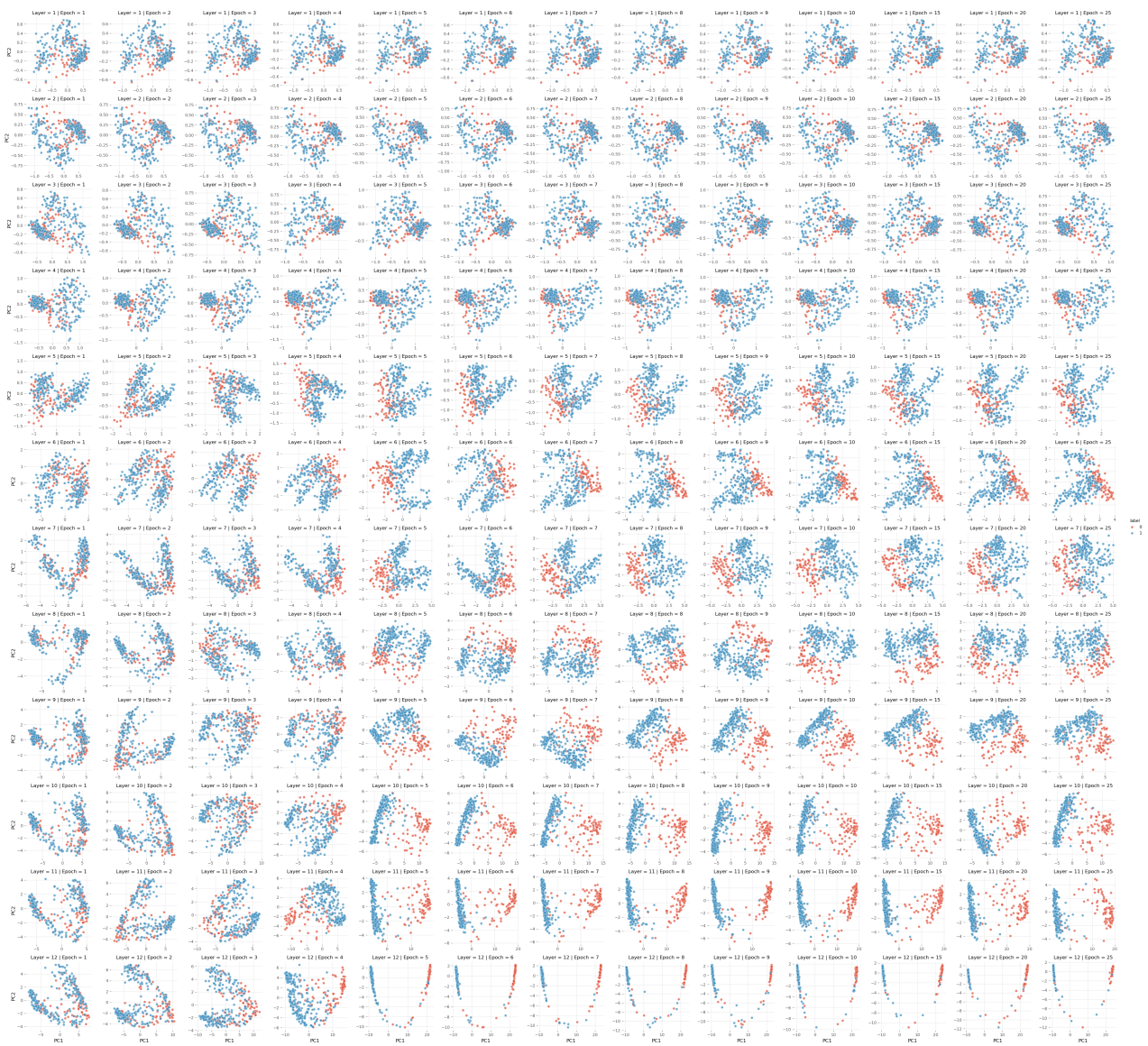


Figure A9: Path-MS: BERT

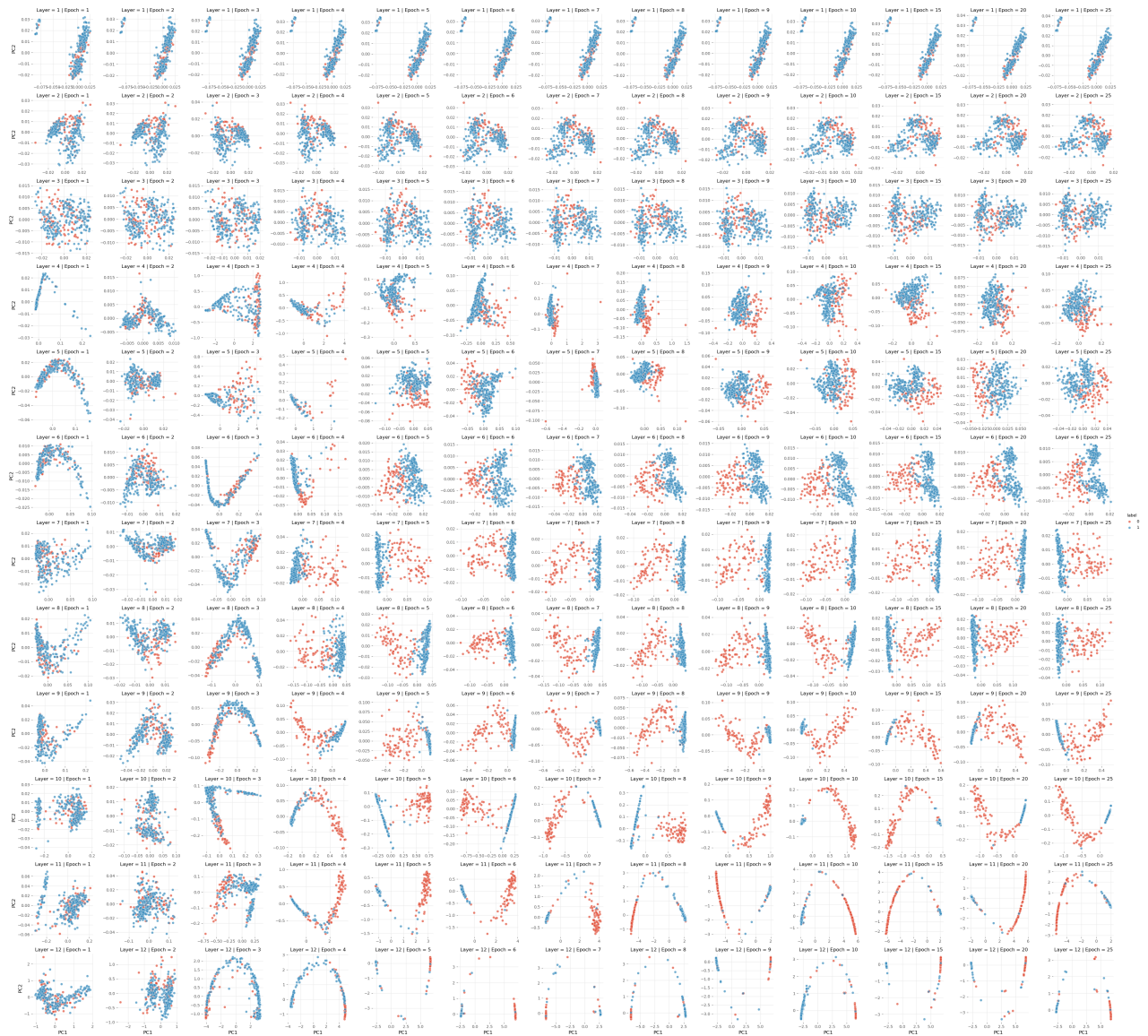


Figure A10: Path-MS: TNLR

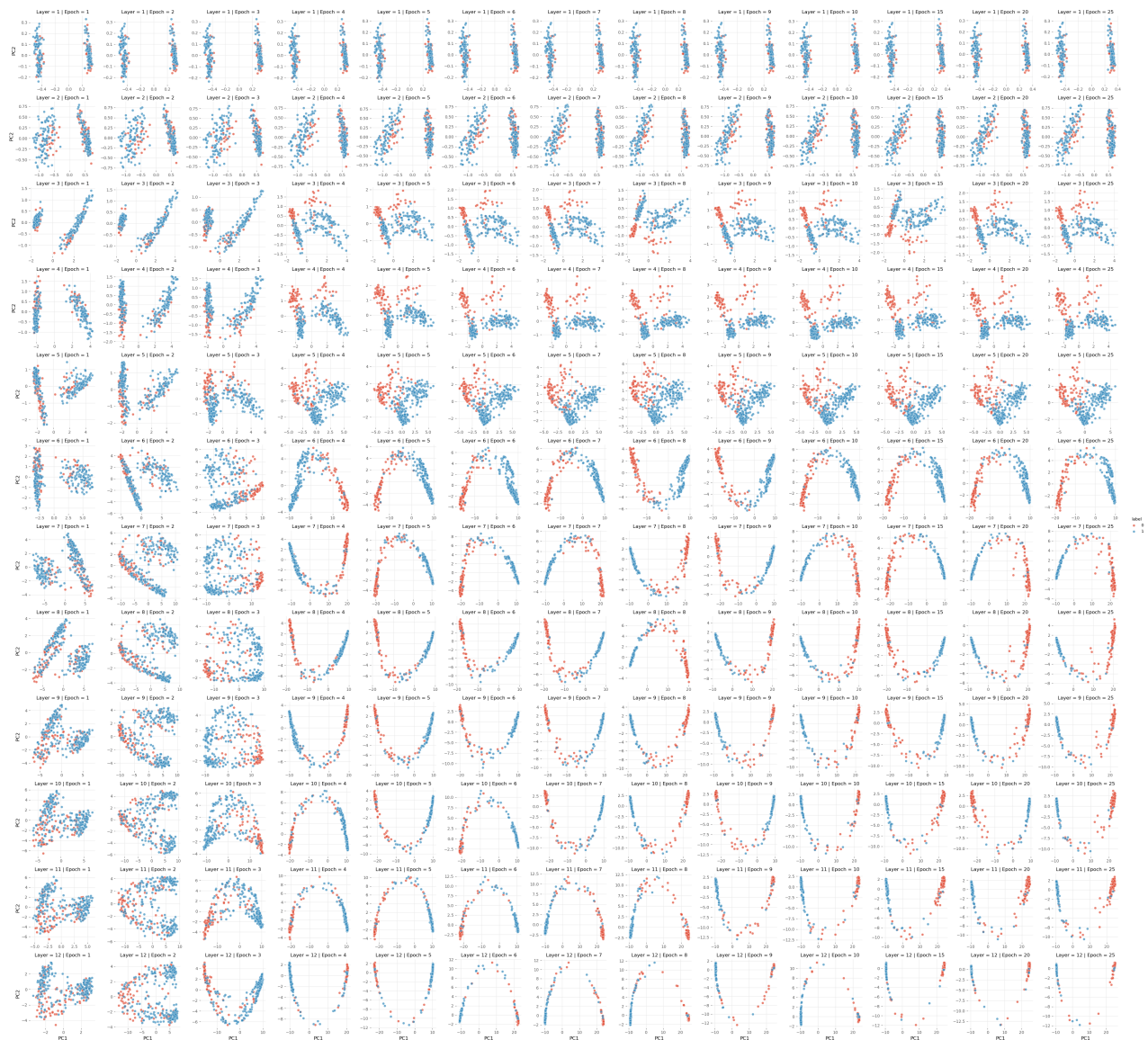


Figure A11: Path-MS: BioBERT



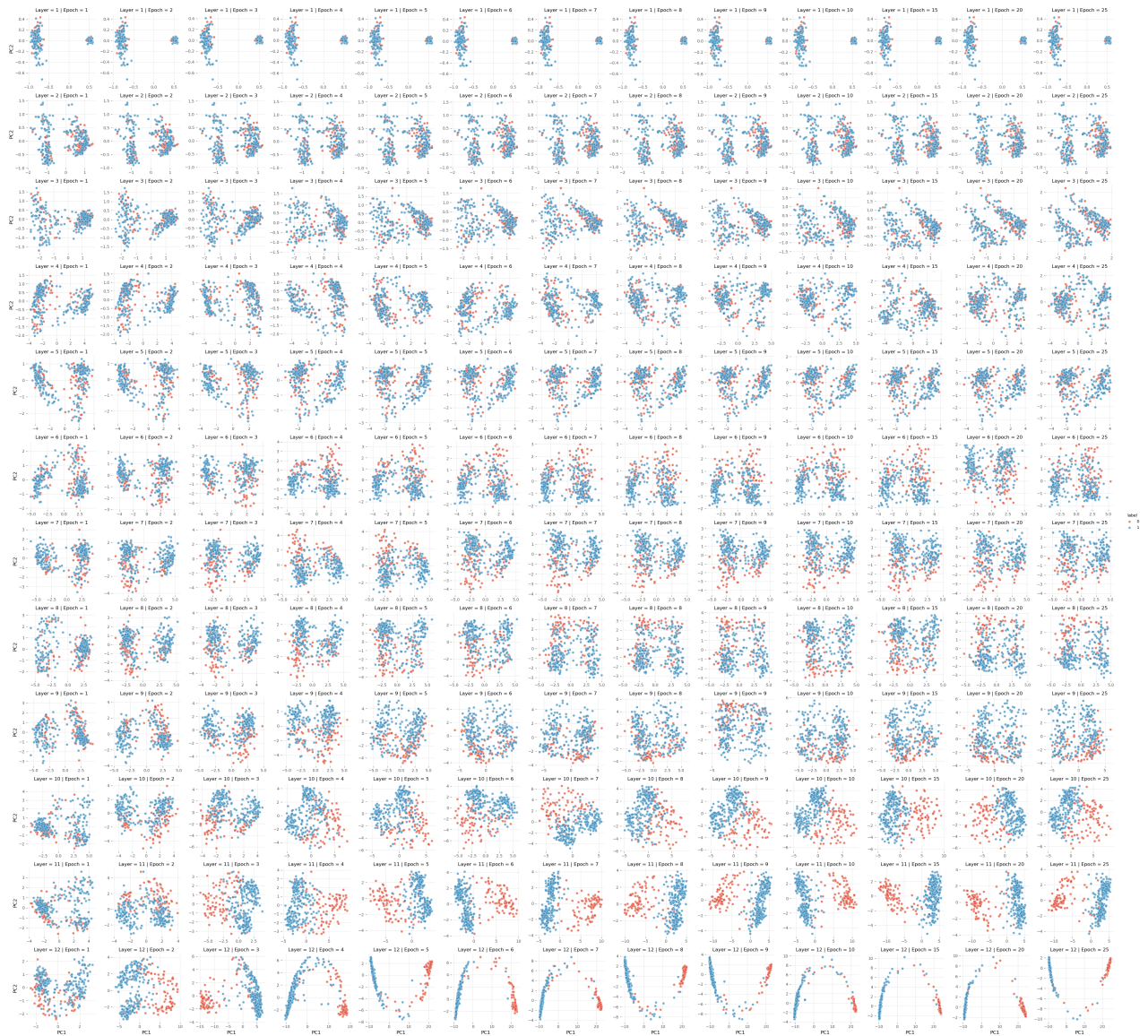


Figure A12: Path-MS: Clinical BioBERT

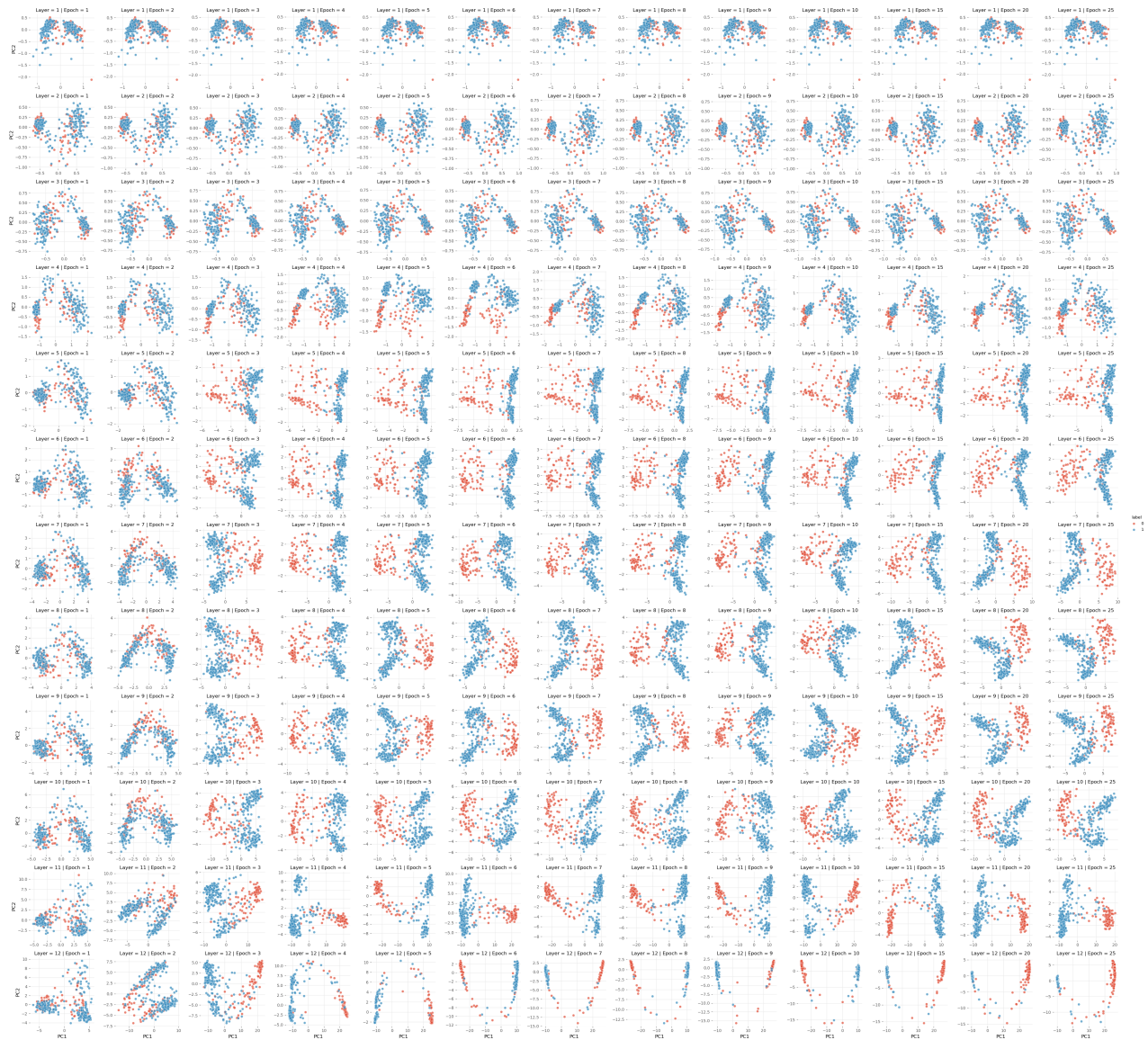


Figure A13: Path-MS: PubMedBERT